12th Brazilian Congress of Manufacturing Engineering
May 10th-12th, 2023, Brasilia, DF, Brazil

# A COMPREHENSIVE EVALUATION OF THE LASER POWER AND POWDER FEED RATE FOR THE DIRECTED ENERGY DEPOSITION PROCESS USING PRINCIPAL COMPONENTS ANALYSIS

**Vincent Edward Wong Diaz**
Mechanical Engineering Department, São Carlos School of Engineering, University of São Paulo
vwong.ufs@gmail.com

**Gustavo Jose Giardini Lahr**
Human-Robot Interfaces and Physical Interaction, Italian Institute of Technology, Genova - Italy.
*gjgl.lahr@gmail.com*

**Glauco Augusto de Paula Caurin**
Aeronautical Engineering Department, São Carlos School of Engineering, University of São Paulo
e-mail: gcaurin@usp.br

**Alessandro Roger Rodrigues**
Mechanical Engineering Department, São Carlos School of Engineering, University of São Paulo
e-mail: roger@sc.usp.br

**Reginaldo Teixeira Coelho**
Production Engineering Department, São Carlos School of Engineering, University of São Paulo
e-mail: rtcoelho@sc.usp.br

***Abstract.*** *Laser Powder Directed Energy Deposition (LP-DED) is a metal manufacturing technique that employs a high-powered laser and powder distribution system. The process begins with the powder transport using an inert gas from the powder distribution system to a coaxial nozzle. Then the powder leaves the coaxial nozzle, and the laser action allows it to melt powder in a substrate to create lines and up layer by layer until creating the final product. The final product's quality heavily depends on the process parameters, which must be adjusted based on the morphology and particle size distribution of each material. These parameters are closely linked to phenomena that occur during the deposition process, such as growth rate, fluid flow in the molten pool, and thermal gradient. Ultimately, these factors determine the mechanical behavior and microstructural features of the final product. One of the challenges observed in the literature is the number of parameters and phenomena involved. These aspects create a multivariate dataset that is difficult to understand from an analytical and experimental point of view. This paper aims to analyze the influence of laser power and powder feed rate on bead geometry using exploratory data analysis and Principal Components Analysis (PCA) to reduce the dataset's dimensionality. To evaluate the deposition quality, we create 49 Single Scan Tracks (SSTs) and then extract four main features: bead height, substrate penetration depth, width, and penetration depth area. The dataset analyzed comprises 194 cross-sections obtained from SSTs containing laser power, powder feed rate, global density energy, line mass, heat input, powder capture efficiency, and dimensional features of cross sections from AISI 316L Single Scan Tracks. Matrix correlation was performed to investigate the relationship of each variable, followed by principal components analysis. The proportion of the total variance showed that two components were sufficient to explain >90% of the dataset. The Random Forest (RF) algorithm was then used to estimate SST quality. PCA improved the model's performance, increasing accuracy from 88% using the original dataset to 91% when principal components were used. This research showed that the geometrical features of SSTs are highly dependent on process parameters. The principal component analysis enabled dimensional reduction to construct relevant features through a linear combination of the original features, improving the dataset's quality and making this approach a useful tool to enhance the performance of machine learning algorithms.*

***Keywords:*** *Laser Powder Directed Energy Deposition; Principal Component Analysis; AISI 316L; Process parameters influence*

## 1. INTRODUCTION

Metal Additive Manufacturing (AM) has emerged as a technology capable of complementing traditional manufacturing methods by creating customizable components (Ko et al., 2015), repairing components (Saboori et al., 2019), and producing parts with complex geometries (Freire et al., 2020). These characteristics have considerably reduced

the fabrication time of high-added value components and low production levels, thereby reducing the impact of GHG emissions in the industrial sector (Saboori et al., 2019). Friel (2015) describes Laser Powder-Directed Energy Deposition (LP-DED) as a Metal AM technique that uses a laser to deposit lines of melted material, which are then layered upon each other to form a final product.

The first step in obtaining high-quality parts using LP-DED is identifying the appropriate process parameters for each material type, morphology, and particle size distribution. These process parameters include Laser Power (LP), Powder Feed Rate (PRF), scanning speed (v), the distance between the nozzle and the substrate, and the amount of gas required to transport the powder and protect the deposition region (Svetlizky et al., 2022). These process parameters create several phenomena during deposition, such as growth rate, fluid flow intensity in the molten pool, and thermal gradient. These factors strongly influence the solidification mode and resulting microstructure (Gao et al., 2022).

Ensuring parts consistency and reliability is a major challenge in the LP-DED process, which requires uniform bead geometries. To achieve optimal process parameters for a new metal powder morphology and particle size distribution, creating Single Scan Tracks (SSTs) is an essential first step (Choi, 2020). Although this procedure minimizes time and cost, a series of SSTs are necessary to find the ideal combination of these process parameters.

When evaluating the cross-section of SSTs, it is possible to extract dimensions such as width, height, penetration depth, penetration depth area, and wetting angle. These measurements allow for evaluating the quality of the bead, including the height-to-width ratio and dilution. The height-to-width ratio reflects the growth of the bead with its width, while dilution is the minimum level of metallurgical bonding required between subsequent layers (Dass & Moridi, 2019). Although the manual calculation of bead quality is possible, this procedure is time-consuming and demands significant assessment time (Borovkov et al., 2021). Thus, alternative automated methods may reduce development time and increase part quality.

Recently, analytical, and numerical approaches have been developed to understand the influence of process parameters on the geometric quality of parts produced using LP-DED. For example, Huang et al. (2019) developed a new physics-based process analytical model that considers residual heat and melt pool bead spreading to estimate the temperature field and predict the final bead geometry. This approach highlights the importance of the powder feed rate in bead height. However, discrepancies between analytical and experimental results have been observed due to powder feeding deviation, neglect of heat convection, and oxidation during the process. Picasso et al. (1994) developed an analytical model considering laser beam velocity and powder feed rate in Laser Cladding. This approach allows for estimating the necessary parameters for cladding deposition by prescribing a height through a series of analytical expressions. One disadvantage, however, is that the track height must be preset, which constrains the influence of process parameters on the bead geometry. Paes et al. (2021) developed a mathematical model to approximate the bead geometry in Inconel 625 and iron, creating multi-layer multi-bead (MLMB) models with experimental validation. The goal was to approximate the experimental bead geometry with the mathematical model.

One drawback of analytical approaches is that they require the simultaneous use of many process parameters during modeling, which increases the complexity of the study and demands more experimental specimens to establish the correlation between analytical and experimental results. At the same time, analytical approaches must make assumptions to minimize the model's complexity. On the other hand, numerical approaches must simplify the computational model to reduce the long processing time and high cost. However, the lack of knowledge of the phenomena during the process limits the accuracy of numerical simulations.

Other studies have focused on monitoring and using sensors to create algorithms that enable the control of process parameters (Song et al., 2012; Meriaudeau & Truchete, 1996; Zhang et al., 2021). This approach has gained relevance, especially in melt pool monitoring, because it provides information during the deposition that regulates specific process parameters such as scanning speed or laser power. This approach is often accompanied by thermocouples, pyrometers, or infrared cameras due to their ability to capture radiation from moving objects without coming into contact with the surface (Zhang et al., 2021). The disadvantage of thermocouples is that they have a relatively low response rate and require contact with the part, making In-situ monitoring difficult to implement. Although pyrometers offer a fast transmission speed, they provide only a single temperature value, so an infrared camera often accompanies them. However, uncertainties and variations that occur during the deposition process, as well as the complexity added by laser reflection and conducted heat, create constraints in melt pool monitoring and information acquisition (Zhang et al., 2021).

Machine Learning (ML) has emerged as a leading method for numerical approaches in LP-DED due to its ability to classify or estimate unknown events with only experimental data. Its applications have included improving part quality (Marko et al., 2022), optimizing process parameters for numerical and experimental models (Meng & Zhang, 2020), and controlling and monitoring the melt pool (Zhang et al., 2021; Quin et al., 2022).

In recent research, Choi (2020) described a methodology for estimating the geometry of SSTs using AISI 316L powder by LP-DED. The study used Multiple Linear Regression, Support Vector Machine, Gradient Boosted Regression, Random Forest, and Artificial Neural Networks to estimate the output parameters of height (S), height (M), and welt angle for SSTs, Multi-tracks, and Cubes. The Artificial Neural Network algorithm had the best performance, with a width of 85.37%, height (S) of 81.59%, height (M) of 96.63%, and welt angle of 54.9%.

Aoyagi et al. (2019) developed a Support Vector Machine (SVM) to construct process maps of cylinder parts in medical CoCr alloys from EB-Powder Bed Fusion, using the speed function and Scan Speed as input parameters. Lim et

al. (2021) used Support Vector Machine with Polynomial kernel, Support Vector Machine-Radial Basis Function and Random Forest algorithms to estimate the surface coloration of titanium alloys from LP-DED. The study analyzed the relationship between coloration, hardness, bead geometry, microstructure, and the percentage of Ti, N, O. The Random Forest algorithm had the best accuracy of 96%, while Support Vector Machine-Radial Basis Function and Support Vector Machine-Polynomial Kernel had accuracies of 85% and 82%, respectively.

This paper aims to analyze the influence of laser power and powder feed rate on bead geometry using exploratory data analysis and improve the performance of the Random Forest algorithm to estimate the quality of the bead, reducing the dimensionality of the dataset by Principal Components Analysis (PCA).

## 2. MATERIALS AND METHODS

### 2.1 Experimental setup

Specimens made of AISI 316L were fabricated via LP-DED using BeAM Machines, Modulo 250. The substrate used had dimensions of 80 mm x 25 mm x 80 mm of AISI 316. Fig. 1 shows the experimental setup, including the components that make up the DED system.

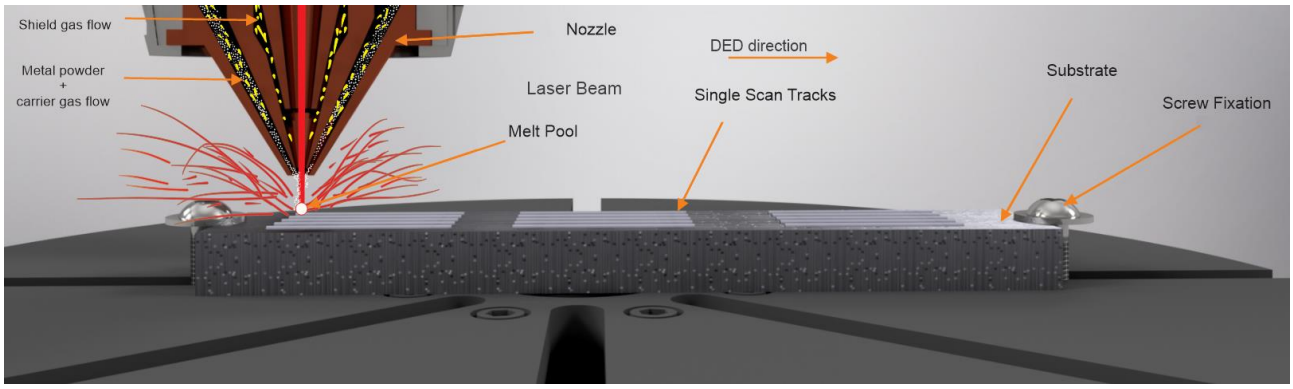


Fig 1. frontal view of the DED system, with nozzle representation that provides powder and argon to the melt pool.

The powder used in the depositions consisted of spherical particles with a size range of 45-105 µm. The powder was produced by Praxair Surface Technologies using vacuum induction melting with argon gas atomization. The powder morphology was analyzed using a 3D laser confocal microscopy LEXT OLS4100 Olympus, and the powder morphology is shown in Fig. 2a. A total of 49 single tracks were deposited to generate the dataset. The laser power ranged between 300 W and 450 W, increasing by 25 W for each deposition. The powder feed rate was set between 5.0 and 8.0 g/min, increasing by 0.5 g/min for each deposited line. The deposition head speed was fixed at 2,000 mm/min, and the argon flow rate in the coaxial head was set at 3 l/min in the central flow, 3 l/min in the carrier flow, and 6 l/min in the shaping flow.

Visual inspection was conducted to determine the optimal conditions for creating SSTs with a linear behavior. SSTs with a stable path and linear deposition were considered Optimal Laser Power (OLP). SSTs that burned along the deposition path were classified as High Laser Power (HLP), while nonlinear beads were categorized as Low Laser Power (LLP). Conventional abrasive cutting was used for metallographic preparation. The beads were cut into four parts, resulting in four cross-sections per bead. The cross-section was sanded with SiC sandpaper up to 2000 mesh and polished in an alumina suspension with 0.3 µm grain size. Chemical etching was performed using Aqua Regia (30 mL HCl, 30 mL HNO3, and 40 mL distilled water) to reveal the microstructure of the deposited AISI 316 L and the substrate. From the bead cross-sections, the metrics width, height, penetration, and dilution area were manually measured using the OLS4100 version 3.1.1 software, as shown in Fig. 2b. The height-width ratio (f) and dilution (d) were calculated using Eq. 1 and Eq. 2, respectively.

$$f = \frac{h}{w} \tag{1}$$

$$d = \frac{p}{h} \tag{2}$$

Regarding bead quality, three criteria were used to evaluate the SSTs. The first criterion was based on visual inspection and categorized as HLP, LLP, or OLP, as described above. The second criterion was the height (h) - length (w) ratio (f), with values between 0.2 and 0.33. The third criterion was the dilution (d), defined as the ratio between the penetration depth (p) and the height (h), with values greater than 10%. The 3D laser confocal microscopy LEXT OLS4100 Olympus was used to construct the dataset for all measurements.

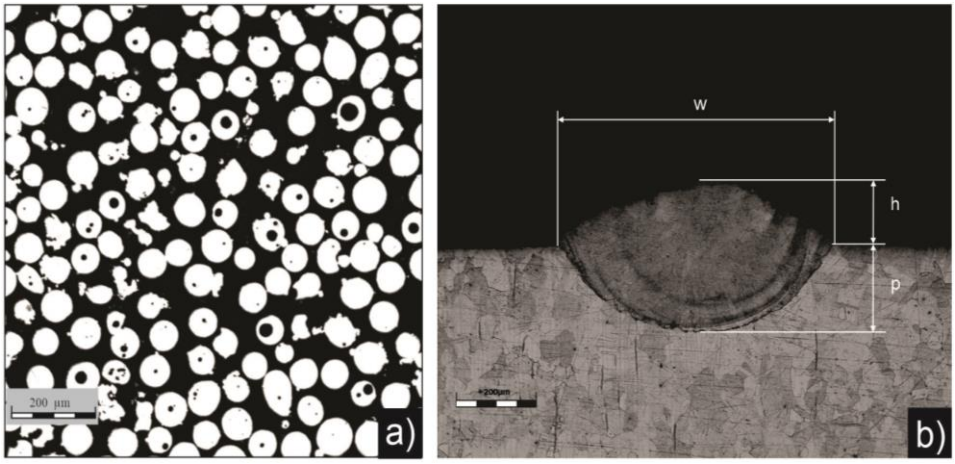


Figure 2. a) Optical microscopy of the metal powder AISI 316L with spherical geometry and the presence of pores and satellites. b) The main features extracted from SSTs are width, height, depth penetration, and the dilution area in a 200 micrometers scale.

Some of the relationships obtained from the process parameters used in this research were:

$$L_m = \dot{M}/V \text{ (g/mm)} \quad (3)$$

$$HI = P/V \text{ (J/mm)} \quad (4)$$

$$\eta = \frac{\rho \cdot V \cdot A_S}{\dot{M}} \quad (5)$$

$$GDE = \frac{P}{\dot{M} \cdot V \cdot d_{beam}^2} \quad \text{(J/(kg/s)·mm}^3\text{)} \quad (6)$$

Where (Lm) is line mass, (Ṁ) is the powder feed rate, (HI) is heat input, (P) is laser power, (V) is deposition speed, η is powder capture efficiency, $A_s$ is the depth penetration area, ρ is the density of AISI 316L, GDE is the global density energy, d is laser spot diameter. Although specific density energy has been used to predict the porosity in LP-DED quantitatively, it does not consider the powder feed rate, which is a critical parameter of LP-DED (Webster et al. 2020). For this reason, the GDE proposed by Webster et al. (2020) was considered in this study.

### 2.2 Principal Components Analysis

The PCA is a statistical technique that linearly transforms a set of p-correlated variables into a set of k uncorrelated variables (with k<p) that explain a substantial portion of the information in the original set (Johnson; Wichern, 2007). The main goal of this approach is to reduce the data dimensionality, obtain a combined interpretation of the original variables, and describe and understand the correlation structure of the original variables.

### 2.3 Random Forest Algorithm

Random forest (RF) is a technique developed by Breiman, (2001). RF can be a collection of classification or regression trees Garcia et al. (2020). This algorithm uses averaging to improve predictive accuracy and control over-fitting. It works as a meta estimator able to divide the data set into a large number of randomly generated decision trees and determine the best decision. One advantage of this technique is the capacity to work with missing values, computing the proximity weighted average of missing values or using median values to replace continuous variables.

## 3. RESULTS AND DISCUSSIONS

A visual evaluation was carried out along the path of each SSTs, and three sets were created: Low Laser Power (LLP), Optimal Laser Power (OLP) and High Laser Power (HLP). During the evaluation, it was observed that laser power values between 400 W and 450 W resulted in burning along the deposition path, while values between 300 W and 325 W showed non-linear scan tracks. The optimal range of laser power was observed between 325 W and 375 W.

The global density energy was analyzed from the laser power and powder feed rate. Increased laser power led to an increase in the global energy density, resulting in larger melt pools. This relationship is expressed by equation 6.

Consequently, large melt pools cause a good powder capture, increasing power efficiency. This phenomenon can be explained by calculating the powder capture efficiency using equation 5 and the laser power categorizations defined above. For LLP, OLP, and HLP, each category's mean powder capture efficiency was 0.052, 0.083, and 0.181, respectively. The increment of powder efficiency capture for each experiment is shown in Fig. 3a.

Another case is when the powder feed rate increases while keeping the laser power constant at 350 W and the scanning speed constant at 2000 mm/min. The global density of energy decreased, as shown in Fig. 3b. We observed experimentally that the height of the bead increased as the global density of energy decreased while the length and width penetration remained the same. This phenomenon was described in recent studies by Figueredo et al. (2021) by calculating the line mass.

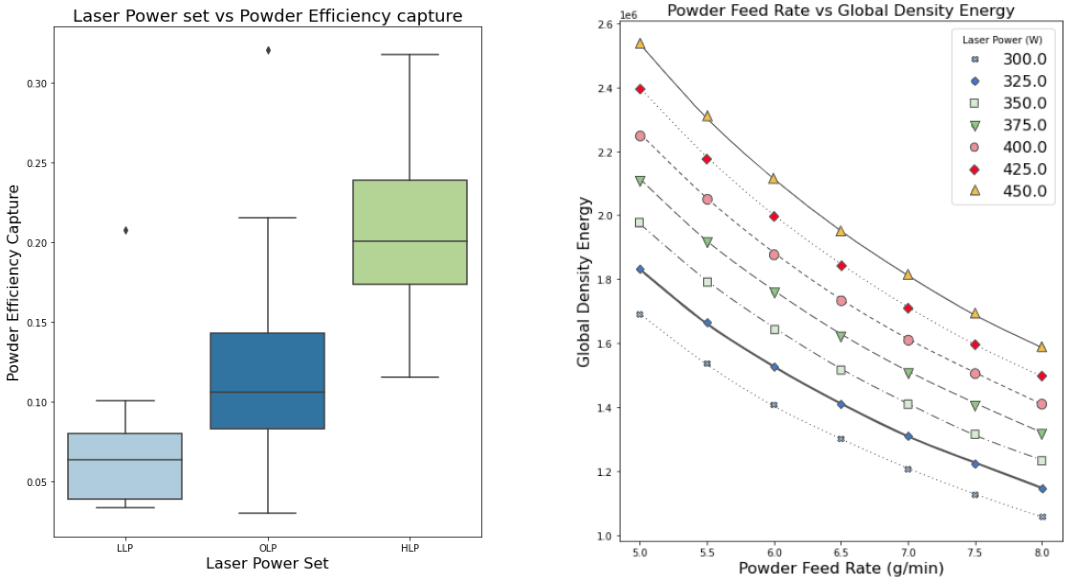


Figure 3: a) Increment of powder efficiency capture from the increment of Laser Power. b) Representation of the powder feed rate vs GDE from the laser power.

An important aspect of evaluating bead geometry is the description of its features. Figure 4a shows the increase in length and width penetration with laser power. The bead height varied between 70 µm and 261.66 µm, with a mean of 152.68 µm and a standard deviation of 38.74 µm.

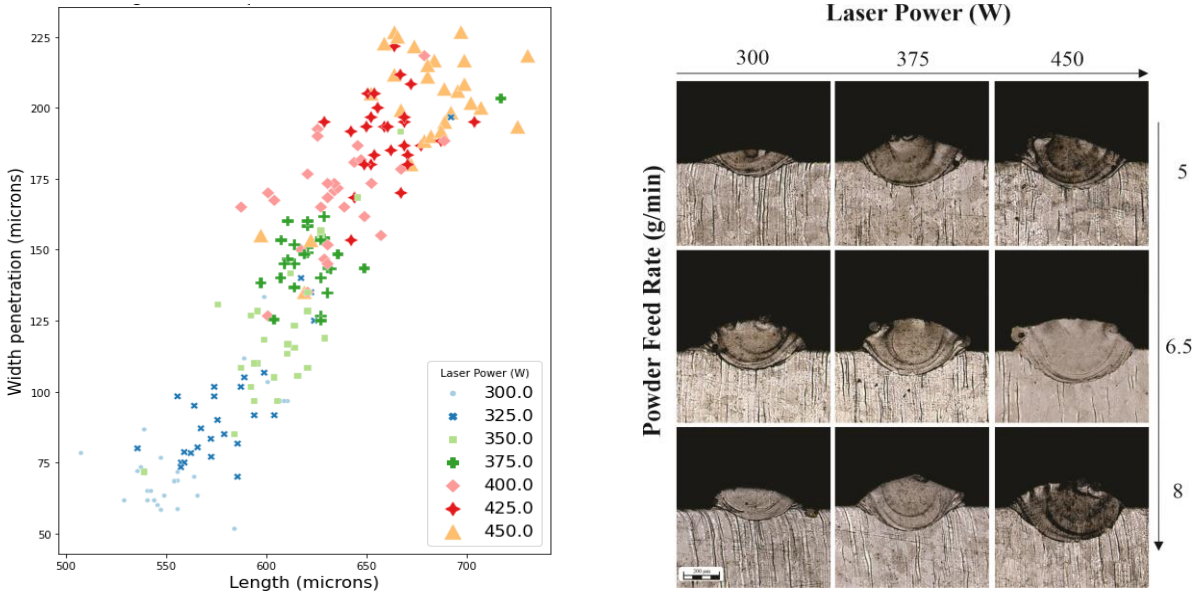


Figure 4 shows (a) the increase in length with the width penetration as the laser power is increased and (b) the variation of bead geometry for different ranges of laser power and powder feed rate.

The length ranged between 507.58 µm and 730.51 µm, with a mean of 621.46 µm and a standard deviation of 45.49 µm. The width penetration ranged from 51.66 µm to 266.68 µm, with a mean of 143.64 µm and a standard deviation of

48.41 µm. Figure 4b illustrates the variation in geometry resulting from the combination of process parameters. Low dilution values indicate poor SST growth, and most of the energy is used for remelting rather than building. By considering the quality criteria described above and searching for the optimal window of powder feed rate, it was observed that the optimal range was between 6.5 g/min and 8.0 g/min in a power range of 325 W to 375 W. At 375 W, the optimal powder feed rate was between 6 g/min and 8 g/min. Equation 1 indicates that 132 cross-sections exhibited a good height-width ratio, representing 68% of the total cross-sections, and all dilutions exhibited a dilution ratio of d>10%.

### 3.1 Principal Components Analysis

The dataset used in this study includes 164 rows and 14 columns. The first six columns represent the process parameters including laser power, powder feed rate and their relationships to the process described in equation (3)(4)(5) and (6). Columns 7 to 10 represent the geometrical dimensions of each bead obtained from the experimental analysis including height, length, depth penetration and depth penetration area. Columns 11 and 12 represent the quality indicators obtained from eq. 1 and 2, respectively. These indicators are assigned values between 0 and 1 to determine if the bead is good quality. Columns 13 and 14 are variables used to categorize laser power and powder feed rate. Table 1 presents the descriptive statistics of the input parameters and the main bead geometry.

Table 1 descriptive statistics of the input parameters and the main bead geometry.

| | Mean | Std | Min | 25% | 50% | 75% | Max |
|---|---|---|---|---|---|---|---|
| LP [W] | 375.64 | 49.96 | 300.00 | 325.00 | 375.00 | 425.00 | 450.00 |
| PFR [g/min] | 6.51 | 0.99 | 5 | 5.5 | 6.5 | 7.5 | 8 |
| Energy density [J/(kg/s)·mm$^3$] | 1.31e2 | 2.75e6 | 8.34e5 | 1.11e5 | 1.28e6 | 1.48e6 | 2.00e6 |
| Heat input [J/mm] | 11.27 | 1.49 | 9.00 | 9.75 | 11.25 | 12.75 | 13.50 |
| Line mass [g/mm] | 0.003 | 0.0005 | 0.002 | 0.002 | 0.003 | 0.003 | 0.004 |
| Efficiency [-] | 0.14 | 0.071 | 0.02 | 0.09 | 0.14 | 0.19 | 0.32 |
| Height [µm] | 152.68 | 38.73 | 69.99 | 128.74 | 153.33 | 179.99 | 261.65 |
| Length [µm] | 621.46 | 45.48 | 507.58 | 592.80 | 620.69 | 653.94 | 730.50 |
| Width penetration [µm] | 143.63 | 48.41 | 51.66 | 101.66 | 148.33 | 186.66 | 226.68 |

A correlation matrix was performed on the first nine columns of the dataset to determine the influence of the process parameters on bead geometry (see Fig. 5). The heatinput showed a high relation with the width penetration (0.9). The global density energy correlated with length (0.56) and width penetration (0.57). The laser power also showed a correlation with the three main bead dimensions: height (0.57), length (0.84), and width penetration (0.9).

The PFR showed a low correlation with the length (-0.034) and did not correlate with the width penetration (0.0). However, it had a moderate correlation with height (0.42). The variance and covariance matrix was used for the PCA, and dimensionality reduction was performed on two principal components. The reduction was based on the proportion of total variance that accounted for over 90% of the original dataset. Several input parameters were considered for the principal component analysis, including LP, PFR, GDE, heat input, line mass, and efficiency.

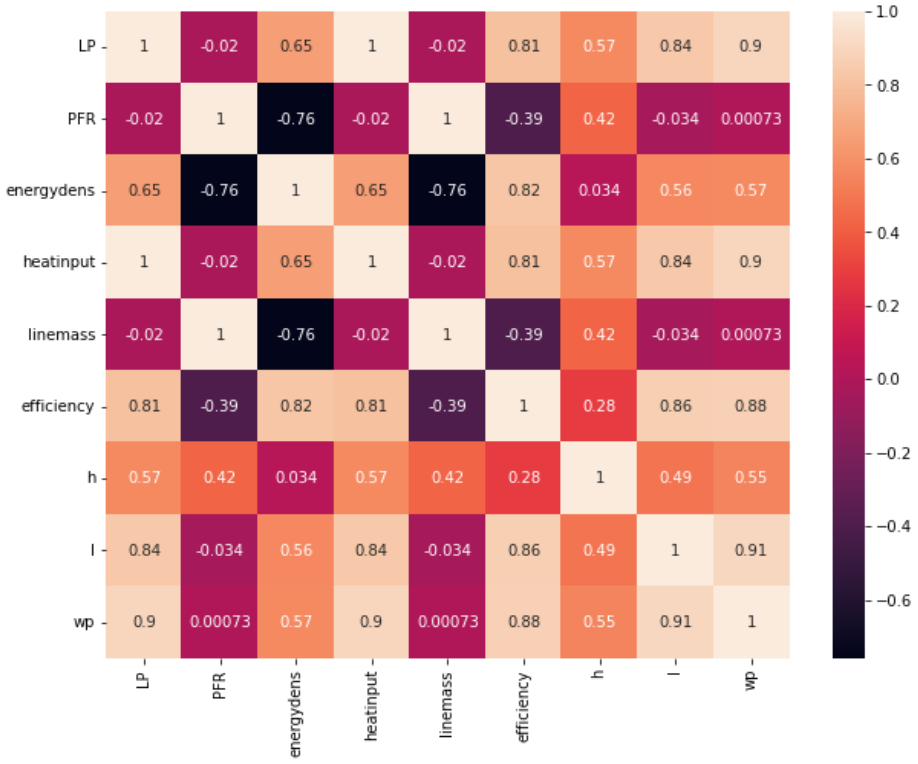


Figure 5. Heatmap of the process parameters with the main bead dimensions

### 3.2 Classification Model

The RF algorithm was implemented as a classifier to estimate the geometrical quality of the bead with five input parameters, and then RF considered the principal components. The hyperparameters of the RF configuration were set as n_estimator = 100, which determines the number of decision trees. We used 70% of the dataset for training and 30% for testing. The precision and recall showed good performance when the original dataset was used. The precision obtained was 89% for identifying bad geometry and 84% for identifying good geometry. The recall of the original dataset was 92% for bad geometries and 79% for identifying good geometries. When summarizing both metrics, the F1 score obtained was 91% for identifying bad geometries and 81% for identifying good geometries. This difference is due to the number of bad geometries compared to good geometries. The accuracy of the original dataset was 88%, as shown in Table 2.

Table 2. Performance comparison of the RF model from the original dataset, and principal components showing an improvement when principal components are used.

| | **RF with the original dataset** | | | | **RF with Principal Components** | | | |
|---|---|---|---|---|---|---|---|---|
| | **Precision** | **Recall** | **F1-score** | **Support** | **Precision** | **Recall** | **F1-Score** | **Support** |
| 0.0 | 0.89 | 0.92 | 0.91 | 64 | 0.89 | 0.98 | 0.93 | 64 |
| 1.0 | 0.84 | 0.79 | 0.81 | 33 | 0.96 | 0.76 | 0.85 | 33 |
| Accuracy | | | 0.88 | 97 | | | 0.91 | 97 |
| Macro avg | 0.87 | 0.85 | 0.86 | 97 | 0.92 | 0.87 | 0.89 | 97 |
| weighted avg | 0.88 | 0.88 | 0.88 | 97 | 0.91 | 0.91 | 0.90 | 97 |

When the principal components were used, an improvement in the main model evaluation metrics was observed, with a 3% increase in accuracy. Precision and recall also showed an improvement when compared with the original dataset.

## 4. CONCLUSIONS

This study aimed to select process parameters for AISI 316L based on visual inspection and geometrical quality using a machine learning algorithm and principal component analysis. The following conclusions were obtained from this research:

Linear deposition, without burns, and a continuous deposition path were observed in the laser power range of 325 W to 375 W. However, laser power higher than 400 W showed burns along the deposition track, and laser power lower than 325 W exhibited a nonlinear deposition path.

Regarding geometry quality, powder feed rate values between 6.5 g/min to 8 g/min, with a laser power of 325 W, displayed a good dilution and height-length ratio. Additionally, powder feed rate values between 5.5 g/min to 8 g/min, with a laser power of 350 W, also exhibited good geometry quality.

Principal Component Analysis (PCA) was used to reduce the dimensionality of the dataset, which improved the accuracy of the Random Forest algorithm in estimating the quality of the beads. Initially, the Random Forest algorithm's accuracy was 88%, but after applying PCA to reduce nine inputs into two components, the model's accuracy increased to 91%. This approach highlights the significance of PCA in enhancing machine learning models and artificial intelligence approaches.

## 5. ACKNOLEDGEMENTS

The authors are thankful to the Coordenação de Aperfeiçoamento de Pessoal de Nível Superior - Brasil (CAPES) - finance code 001 and the São Paulo Research Foundation (FAPESP) for funding the research through the grant process n. 2019/00343-I. Also, the authors are grateful to Fabio Edson Mariani's assistance in cutting and hot forming the samples.

## 6. REFERENCES

Aoyagi, K., Wang, H., Sudo, H., & Chiba, A. 2019. Simple method to construct process maps for additive manufacturing using a support vector machine. *Additive Manufacturing*, Vol. *27*, p. 353–362.

Borovkov, H., de la Yedra, A. G., Zurutuza, X., Angulo, X., Alvarez, P., Pereira, J. C., & Cortes, F. 2021. In-Line Height Measurement Technique for Directed Energy Deposition Processes. *Journal of Manufacturing and Materials Processing*, Vol. *5*(3), p. 85.

Breiman, L. 2001. Random Forests. *Machine Learning*, Vol. *45*(1), p. 5–32.

Choi, T.-Y. 2020. *Machine learning based predictive modeling of dimensional quality in direct energy deposition with SUS316L*

Dass, A., & Moridi, A. 2019. State of the Art in Directed Energy Deposition: From Additive Manufacturing to Materials Design. *Coatings*, Vol. *9*(7). p. 418

Paes, L. E., Ferreira, H. S., Pereira, M., Xavier, F. A., Weingaertner, W. L., & Vilarinho, L. O. 2021. Modeling layer geometry in directed energy deposition with laser for additive manufacturing. *Surface and Coatings Technology*, Vol. *409*, p. 126897.

Figueredo, E. W. A., Apolinario, L. H. R., Santos, M. v, Silva, A. C. S., Avila, J. A., Lima, M. S. F., & Santos, T. F. A. 2021. Influence of Laser Beam Power and Scanning Speed on the Macrostructural Characteristics of AISI 316L and AISI 431 Stainless Steel Depositions Produced by Laser Cladding Process. *Journal of Materials Engineering and Performance*, vol. *30*(5), p. 3298–3312.

Freire, B., Babcinschi, M., Ferreira, L., Señaris, B., Vidal, F., & Neto, P. 2020. Direct Energy Deposition: a complete workflow for the additive manufacturing of complex shape parts. *Procedia Manufacturing*, vol. *51*, p. 671–677.

Friel, R. J. 2015. 13 - Power ultrasonics for additive manufacturing and consolidating of materials. In J. A. Gallego-Juárez & K. F. Graff (Eds.), *Power Ultrasonics* p. 313–335.

Gao, S., Feng, Y., Wang, J., Qin, M., Bodunde, O. P., Liao, W.-H., & Guo, P. 2021. Molten pool characteristics of a nickel-titanium shape memory alloy for directed energy deposition. *Optics & Laser Technology*, vol. *142*, p. 107215.

García-Moreno, A.-I., Alvarado-Orozco, J.-M., Ibarra-Medina, J., & Martínez-Franco, E. 2020. Image-based porosity classification in Al-alloys by laser metal deposition using random forests. *The International Journal of Advanced Manufacturing Technology*, vol. *110*(9–10), p. 2827–2845.

Huang, Y., Khamesee, M. B., & Toyserkani, E. 2019. A new physics-based model for laser directed energy deposition (powder-fed additive manufacturing): From single-track to multi-track and multi-layer. *Optics & Laser Technology*, vol. *109*, p. 584–599.

Johnson, R.,Wichern D., 2007. Applied Multivariate Statistical Analysis. Prentice Hall, 6th edition.

Ko, H., Moon, S. K., & Hwang, J. 2015. Design for additive manufacturing in customized products. *International Journal of Precision Engineering and Manufacturing*, vol. *16*(11), p. 2369–2375.

Lim, J.-S., Oh, W.-J., Lee, C.-M., & Kim, D.-H. 2021. Selection of effective manufacturing conditions for directed energy deposition process using machine learning methods. *Scientific Reports*, vol. *11*(1), p. 24169.

Marko, A., Bähring, S., Raute, J., Biegler, M., & Rethmeier, M. 2022. Quality Prediction in Directed Energy Deposition Using Artificial Neural Networks Based on Process Signals. *Applied Sciences*, vol. *12*(8), p. 3955.

Meriaudeau, F., & Truchetet, F. 1996. Control and optimization of the laser cladding process using matrix cameras and image processing. *Journal of Laser Applications*, vol. *8*(6), p. 317–324.

Meng, L., & Zhang, J. 2020. Process Design of Laser Powder Bed Fusion of Stainless Steel Using a Gaussian Process-Based Machine Learning Model. *JOM*, vol. *72*(1), p. 420–428.

Picasso, M., Marsden, C. F., Wagniere, J. D., Frenk, A., & Rappaz, M. 1994. A simple but realistic model for laser cladding. *Metallurgical and Materials Transactions B*, vol. *25*(2), p. 281–291.

Quin, J., Hu, F., Liu, Y., Witherell, P., Wang, C. C. L., Rosen, D. W., Simpson, T. W., Lu, Y., & Tang, Q. 2022. Research and application of machine learning for additive manufacturing. *Additive Manufacturing*, vol. *52*, p. 102691.

Song, L., Bagavath-Singh, V., Dutta, B., & Mazumder, J. 2012. Control of melt pool temperature and deposition height during direct metal deposition process. *The International Journal of Advanced Manufacturing Technology*, p. *58*(1–4), p. 247–256.

Saboori, A., Aversa, A., Marchese, G., Biamino, S., Lombardi, M., & Fino, P. 2019. Application of Directed Energy Deposition-Based Additive Manufacturing in Repair. *Applied Sciences*, Vol. *9*(16). p. 3316.

Svetlizky, D., Zheng, B., Steinberg, D. M., Schoenung, J. M., Lavernia, E. J., & Eliaz, N. 2022. The influence of laser directed energy deposition (DED) processing parameters for Al5083 studied by central composite design. *Journal of Materials Research and Technology*, vol. *17*, p. 3157–3171.

Webster, S., Ehmann, K., & Cao, J. 2020. Energy Density Comparison via High speed, In-situ Imaging of Directed Energy Deposition. *Procedia Manufacturing*, vol. *48*, p. 691–696.

Zhang, Z., Liu, Z., & Wu, D. 2021. Prediction of melt pool temperature in directed energy deposition using machine learning. *Additive Manufacturing*, vol. *37*, p. 101692.

## 7. RESPONSIBILITY NOTICE

The authors are the only responsible for the printed material included in this paper.